Available online at www.sciencedirect.com

ScienceDirect

Ceramics International 40 (2014) 501–509

CERAMICS INTERNATIONAL

www.elsevier.com/locate/ceramint

The structure and in vitro apatite formation ability of porous titanium covered bioactive microarc oxidized TiO_2-based coatings containing Si, Na and Ca

Rui Zhou[a], Daqing Wei[a,*], Su Cheng[b], Baoqiang Li[a], Yaming Wang[a], Dechang Jia[a], Yu Zhou[a], Haifeng Guo[a]

[a]*Institute for Advanced Ceramics, Department of Materials Science and Engineering, Harbin Institute of Technology, Harbin 150001, PR China*
[b]*Department of Mechanical Engineering, School of Architecture and Civil Engineering, Harbin University of Science and Technology, Harbin 150001, PR China*

Received 15 May 2013; accepted 9 June 2013
Available online 17 June 2013

Abstract

The microarc oxidation (MAO) was used to prepare TiO_2 based coating containing Si, Ca and Na elements (SCN) on porous titanium sintered with different sizes of titanium beads. The chemical states of elements and apatite-forming ability of MAO coatings were investigated. The effect of titanium beads diameter on the chemical states of Ca and Si of MAO coatings on the surfaces of porous titanium is not obvious. However, the chemical states of Ti and O changed when the titanium beads diameter increased. The current results reveal that the MAO coatings containing SCN elements have good induction capability for the heterogeneous nucleation and growth of apatite in a simulated body fluid (SBF). The appropriate size of titanium beads could promote the apatite formation on porous titanium with MAO coatings. The reason for this is that the appropriate size of titanium beads can be helpful to introduce more amounts of SCN elements into MAO coatings on the porous titanium.

Keywords: D. Apatite; Coatings; Microarc oxidation; Porous titanium

1. Introduction

As far as structural and mechanical compatibility is concerned, porous materials are suitable for application in bone replacement and bone restoration, because they conquer the shortage of mismatch of Young's modulus between materials and bone [1–3]. Among various metallic biomaterials, Ti and its alloys are most widely used as their excellent corrosion resistance and biocompatibility properties [4,5]. Meanwhile, a number of approaches have been investigated to fabricate three-dimensionally porous titanium, such as partial sintering of powders [6] or wires [7], sintering of powders around a temporary space-holding phase [8,9], and selective laser or electron beam melting technique [10–12]. Hence, it is noticeable that Ti shows poor osteoinductive properties caused by bioinert in its application, and this limits its further application [13–15]. Microarc oxidation is a relatively convenient and effective technique to solve this problem, as desired elements and various functional coatings can be fabricated on the substrate by adjusting the electrolyte [16–20]. Thus, MAO technique has received much attention in recent years [21–27], but most MAO coatings were formed on the flat substrates, and the researches in the formation of MAO coatings on the porous titanium have less reported.

In our recent works [28], porous titanium was prepared by vacuum sintering titanium beads with diameters of 100, 200, 400 and 600 μm on titanium plate at temperature 1723 K for 2 h. Then TiO_2-based coatings containing Si, Ca, Na (SCN) elements were fabricated by micro-arc oxidation (MAO) on the porous titanium. The results showed that the surface

*Correspondence to: Institute for Advanced Ceramics, Department of Materials Science and Engineering, Harbin Institute of Technology, Yikuang Street, Harbin 150001, P.O.Box 3022#, PR China.
Tel.: +86 451 8640 2040 8403; fax: +86 451 8641 4291.
E-mail address: daqingwei@hit.edu.cn (D. Wei).

0272-8842/$ - see front matter © 2013 Elsevier Ltd and Techna Group S.r.l. All rights reserved.
http://dx.doi.org/10.1016/j.ceramint.2013.06.030

morphology, SCN concentrations and X-ray diffraction intensity of titania of the MAO coatings were significantly affected by titanium beads diameter. The porosity and specific surface area are two key factors to influence the formation and microstructures of MAO coatings [28]. The further investigation indicated that the interior of the porous titanium could be coated by MAO coatings. However, it is not clear up to now that the structure such as elemental chemical states and apatite formation of MAO coatings on the porous titanium. Moreover, the previous research indicated that the oxidizing ability is positive correlated with bead diameter as porosity but negative correlated with bead diameter as specific surface area, which could further affect the formation of apatite on the MAO coating. Thus, it was necessary for investigating the apatite formation of MAO treated porous titanium, and exhibiting clearly the formation and characters of apatite on the MAO coating.

2. Experimental procedure

2.1. Specimens preparation

Four kinds of commercial titanium beads with diameters of 100, 200, 400 and 600 μm supplied by Baoji Haibao special metal materials Co. Ltd., of China were sintered to fabricate porous titanium. Fig. 1 shows the scahemtic diagram for the structure of the porous titanium prepared by vacuum sintering titanium beads. The porous Ti layer with thickness of 0.4–0.6 mm were prepared by using titanium beads to be sintered on titanium plates ($30 \times 30 \times 1\ mm^3$), where the titanium plates were ground with 400#, 800# and 1000# abrasive papers, washed with acetone and distilled water, and dried at 40 °C. The Ti plates covered by titanium beads with four different particle sizes were filled in a graphite mold. BN lubricant was sprayed on the inner wall of the mold to avoid the reaction between graphite and Ti during sintering. At last, the samples were sintered under vacuum environment (10^{-3} Pa) without applied pressure by holding at temperature 1723 K for 2 h with a heating rate of 10 °C/min.

Table 1 shows the sample labels and diameter of titanium beads. The Ti plates covered titanium beads were used as anodes, and stainless steel plates were used as cathodes in an electrolytic bath. An electrolyte was prepared by the dissolution of reagent-grade chemicals of $Ca(CH_3COO)_2 \cdot H_2O$ (6.3 g/l), Na_2SiO_3 (13.2 g/l), EDTA-2Na (15 g/l) and NaOH (15 g/l) into deionized water. The applied voltage of 500 V was used to prepare MAO coatings on substrates. The frequency, duty cycle and oxidizing time were 600 Hz, 8.0% and 5 min respectively. The temperature of the electrolyte was kept at 40 °C by cooling system.

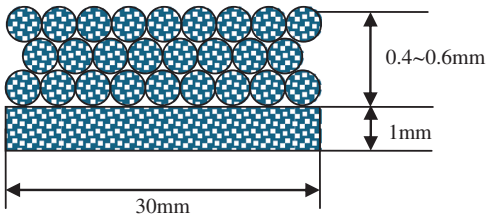

Fig. 1. Schematic diagram for the structure of the porous titanium prepared by vacuum sintering titanium beads on titanium plate.

Table 1
The sample labels and diameter of titanium beads.

Labels	Diameter of titanium beads (μm)
MAO100	100
MAO200	200
MAO400	400
MAO600	600

Table 2
Ion concentrations of the SBF and human blood plasma.

Ion	Concentrations (mmol/l)	
	SBF	Blood plasma
Na^+	142.0	142.0
K^+	5.0	5.0
Mg^{2+}	1.5	1.5
Ca^{2+}	2.5	2.5
Cl^-	147.8	103.8
HCO_3^{2-}	4.2	27
HPO_4^{2-}	1.0	1.0
SO_4^{2-}	0.5	0.5

2.2. Immersion of the samples in a simulated body fluid

The MAO treated porous titanium was soaked in 15 mL simulated body fluid (SBF) (Table 2), immersing for different time, and the SBF was refreshed every other day. The SBF was prepared by dissolving reagent-grade chemicals of NaCl, $NaHCO_3$, KCl, $K_2HPO_4 \cdot 3\ H_2O$, $MgCl_2 \cdot 6\ H_2O$, $CaCl_2$, and Na_2SO_4 into deionized water and buffering at pH 7.40 with tris-hydroxymethylaminomethane ($(CH_2OH)_3CNH_2$) and 1.0 mol/L HCl at 37 °C [29].

2.3. Structure characterization

2.3.1. X-ray diffraction (XRD)

The phase composition of MAO samples after SBF immersion were analyzed by X-ray diffraction (XRD, D/max-gB, Japan) using a Cu Kα radiation with a continuous scanning mode at a rate of 4°/min, under an accelerating voltage of 40 kV and current of 50 mA.

2.3.2. Scanning electron microscopy (SEM) and energy dispersive X-ray spectrometer (EDS)

Scanning electron microscopy (SEM, Quanta 200, FEI Co., American) was used to observe the surface morphologies. In addition, the elemental concentrations of the surface of samples were detected by an energy dispersive X-ray spectrometer (EDS, EDAX, American) equipped on the SEM system.

2.3.3. X-ray photoelectron spectroscopy

An X-ray photoelectron spectroscopy (XPS, K-Alpha, Thermofisher Scienticfic Co., American) was used to detect the chemical compositions of the coating surfaces. In the XPS experiment, an AlKα (1486.6 eV) X-ray source was used for the XPS work under a vacuum of 1.0×10^{-8} mbar. The current of X-ray beam was 6 mA and the resolution for energy was 0.5 eV with a scanning step of 0.1 eV. The regions of 400 μm^2 on the sample surfaces were analyzed. The measured binding energies were calibrated by the C1s (hydrocarbon C–C, C–H) of 285 eV. And the chemical states of various elements before and after Ar^+ ions etching for 60 s were analyzed.

2.3.4. Fourier transform infrared spectroscopy

Fourier transform infrared spectroscopy (FT-IR, Magna-IR 560 E.S.P., American) was used to analyze the apatite structure. In the FT-IR experiment, the scanning range and resolution were 4000–400 and 4 cm^{-1}, respectively. Approximately 1 mg of apatite layer on the samples mixed with about 500 mg of dry KBr powder was ground using an agate mortar and pestle. The mixed powder was pressed into transparent disks with a diameter of 13 mm for the FT-IR work.

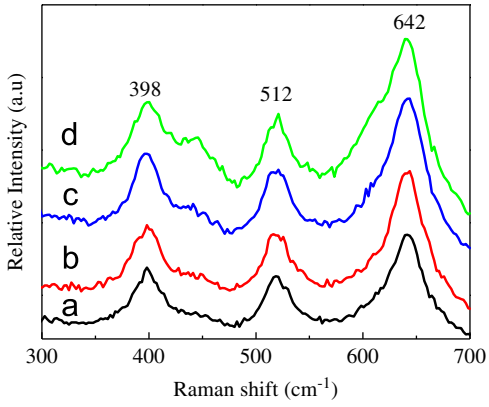

Fig. 2. Raman spectra of the SC coating on porous titanium prepared by sintering titanium beads with different diameters: (a) MAO100, (b) MAO200, (c) MAO400, and (d) MAO600.

3. Results and discussion

3.1. Structure of MAO coatings

3.1.1. Raman spectra of MAO coatings

Fig. 2 shows the Raman spectra of the MAO coating. Peaks at 400, 512 and 642 cm^{-1} indicated the formation of TiO_2 in the MAO coatings.

3.1.2. XPS of MAO coatings

In this work, the major surface constituents of the MAO coatings formed porous titanium prepared by sintering titanium beads with different diameters before and after etching. Fig. 3 shows the XPS survey of MAO coatings before and after etching. The major surface constituents found for the MAO coatings are Si, Ca, Ti, O, Na and C. Before etching, the C1s peak was obviously higher compared to the etched samples due to the environmental contamination. Correspondingly, the Ca2p, Ti2p and Si2p peaks increased due to the removing of contaminated C after etching.

Fig. 4 shows the atomic concentration ratios of O/Ti, Ca/Ti and Si/Ti according to XPS results of the MAO coatings formed porous titanium prepared by sintering titanium beads with different diameters before and after etching. Generally, the change in O/Ti, Ca/Ti and Si/Ti with increasing the titanium beads diameter is similar before and after etching. And it was obviously that the O/Ti, Ca/Ti and Si/Ti increased firstly when the titanium beads diameter increasing from 100 to 400 μm and then they decreased when further increasing the titanium beads diameter to 600 μm. These results indicated that the titanium beads diameter has significant effects on the atomic concentrations of O/Ti, Ca/Ti and Si/Ti.

Fig. 5 shows the XPS high-resolution spectra of Ca2p of MAO coatings on porous titanium prepared by sintering titanium beads with different diameters. Before etching, the Ca2p spectrum revealed a doublet of $Ca2p_{3/2}$ and $Ca2p_{1/2}$ at binding energy of 347.4 and 351.1 eV as shown in Fig. 5(a), corresponding to Ca^{2+} [30]. After etching, the Ca2p spectra show similar curves of the samples before etching (Fig. 5b).

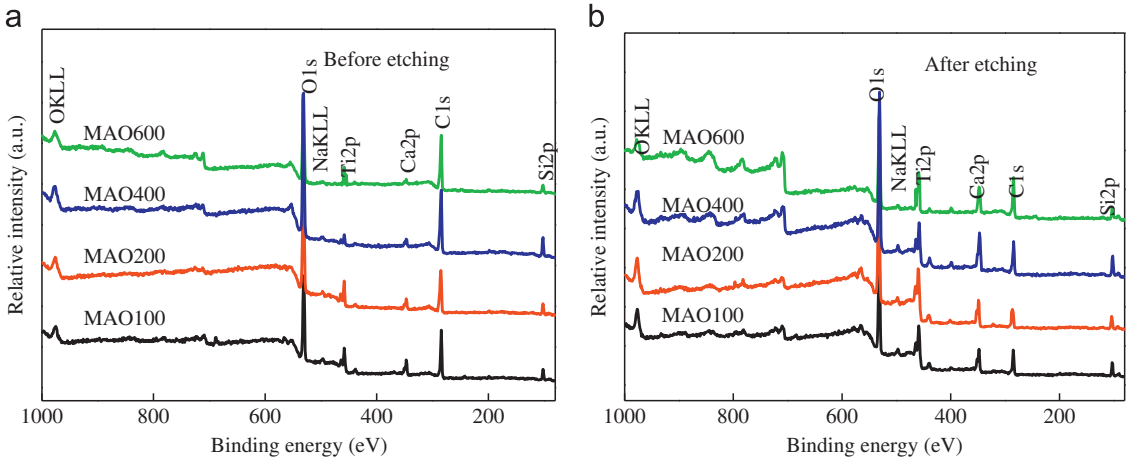

Fig. 3. XPS survey of the MAO coatings formed porous titanium prepared by sintering titanium beads with different diameters: (a) before etching and (b) after etching.

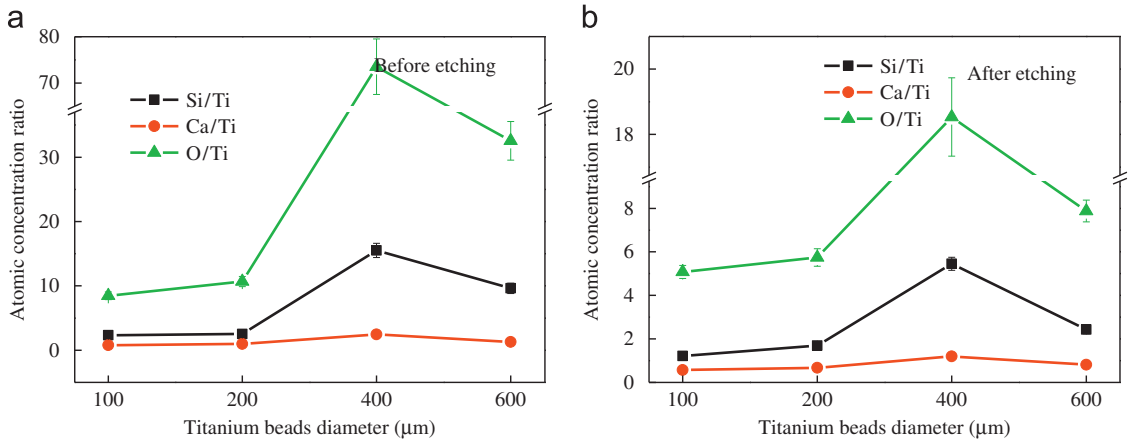

Fig. 4. Atomic concentration ratios of O/Ti, Ca/Ti and Si/Ti according to XPS results of the MAO coatings formed porous titanium prepared by sintering titanium beads with different diameters: (a) before etching and (b) after etching.

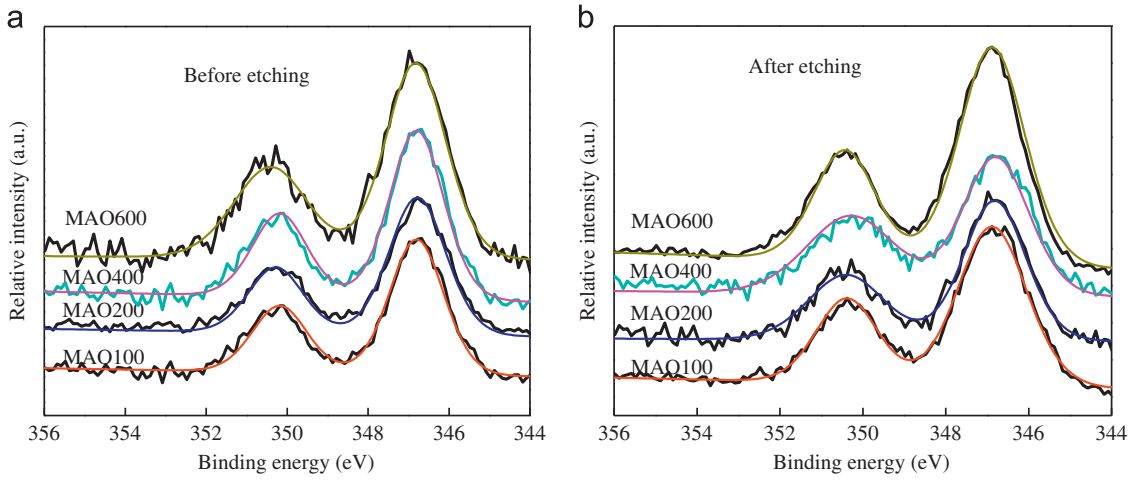

Fig. 5. XPS high-resolution spectra of Ca2p of the MAO coatings on porous titanium prepared by sintering titanium beads with different diameters: (a) before etching and (b) after etching.

Fig. 6 shows the XPS high-resolution spectra of Si2p of MAO coatings on porous titanium prepared by sintering titanium beads with different diameters. Before and after etching, the Si2p spectrum revealed the binding energy of Si2p at 102.4 eV, corresponding to Si^{4+}.

Fig. 7 shows the Ti2p and O1s spectra of the MAO coatings on porous titanium prepared by sintering titanium beads with different diameters. The Ti2p peaks were asymmetric, indicating high and low valences of Ti. The Ti2p could be fitted by high binding energy at 458.5 ± 0.2 eV corresponding to Ti^{4+} and low binding energy at 457.6 ± 0.2 eV corresponding to Ti^{2+} [31], indicating the presence of TiO_2 and TiO in the coatings. In addition, it was observed the peaks intensity at 457.6 ± 0.2 eV decreased when increasing the titanium beads diameter from 100 to 400 μm and then they rose when further increasing the titanium beads diameter to 600 μm. In Fig. 7(b), the O1s spectra also show an asymmetric form similar to Ti2p. They could be fitted with two components including high binding energy of 532.3 ± 0.2 eV attributed to TiO and low binding energy of 531.5 ± 0.2 eV assigned to TiO_2 and/or other oxides containing silicon or calcium. And the peaks intensity at 532.3 ± 0.2 eV decreased when increasing the titanium beads diameter from 100 to 400 μm and then they rose when further increasing the titanium beads diameter to 600 μm.

Fig. 8 shows the intensity ratios between high binding energy and low binding energy of Ti2p and O1s. Evidently, the change in the intensity ratio between high binding energy/low binding energy of Ti2p increased when increasing the titanium beads diameter from 100 to 400 μm and then they rose when further increasing the titanium beads diameter to 600 μm. However, the change in that of O1s is contrary to Ti2p. These results indicated that the titanium beads diameter has significant effects on the chemical states of Ti2p and O1s.

3.2. Apatite formation ability of MAO coatings

3.2.1. XRD of MAO coatings after SBF immersion

Fig. 9 shows the XRD patterns of the MAO coating formed at the surfaces of porous titanium beads with different diameters after SBF immersion for 14 days. Apparently, the diffraction peaks of apatite were detected, indicating the MAO

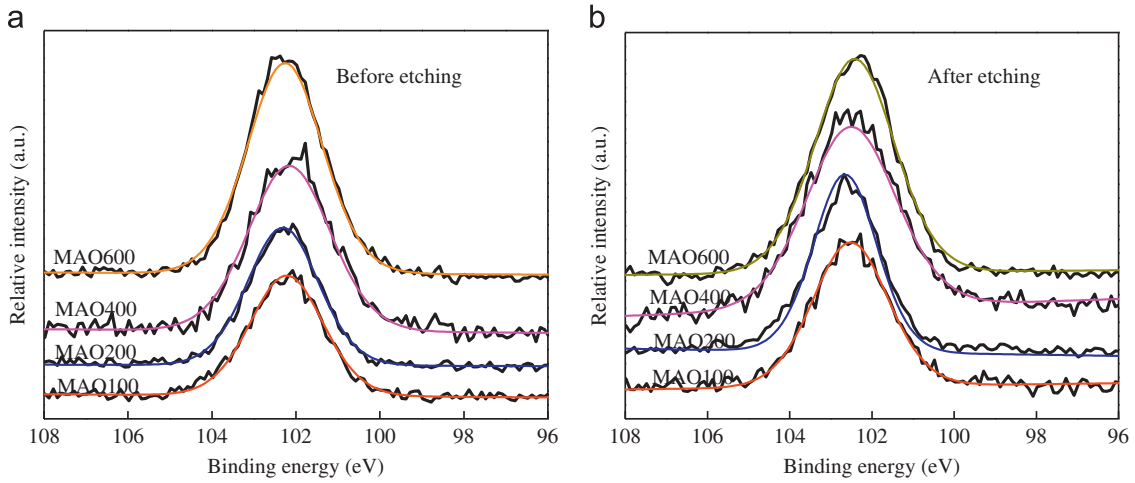

Fig. 6. XPS high-resolution spectra of Si2p of the MAO coatings on porous titanium prepared by sintering titanium beads with different diameters: (a) before etching and (b) after etching.

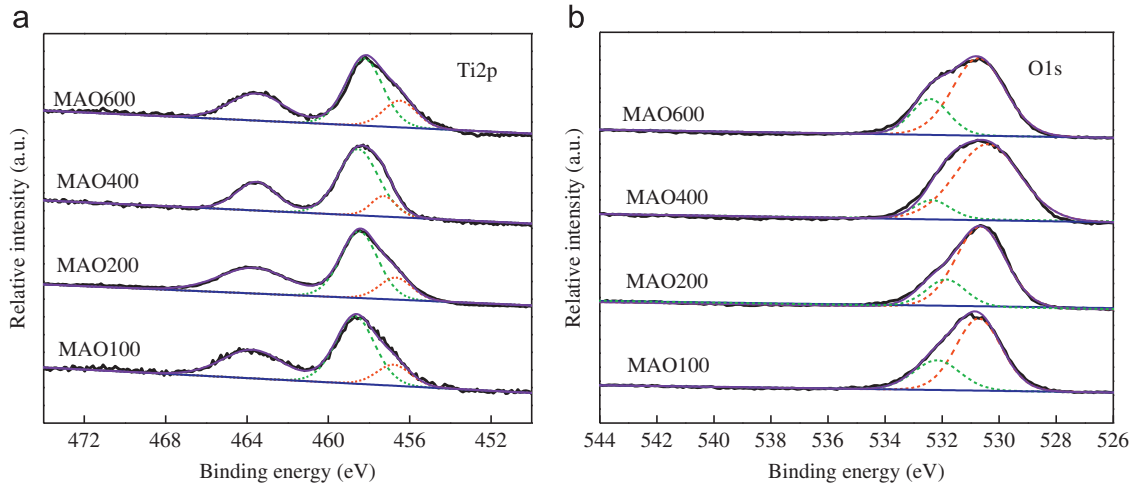

Fig. 7. XPS high-resolution spectra of Ti2p and O1s of the MAO coatings on porous titanium prepared by sintering titanium beads with different diameters after etching: (a) Ti2p and (b) O1s.

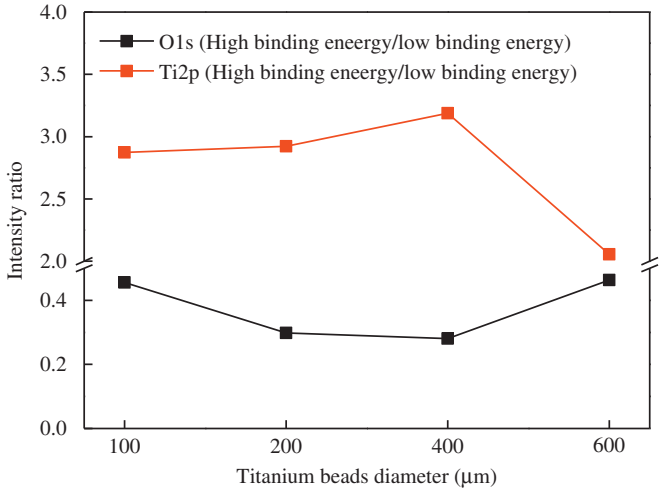

Fig. 8. The intensity ratios between high binding energy and low binding energy of Ti2p and O1s.

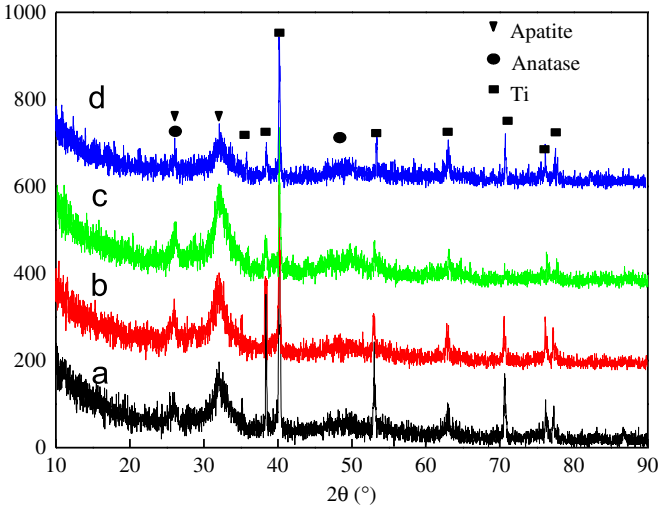

Fig. 9. XRD patterns of the MAO coating formed at the surfaces of porous titanium beads with different diameters after SBF immersion for 14 days: (a) MAO100, (b) MAO200, (c) MAO400, and (d) MAO600.

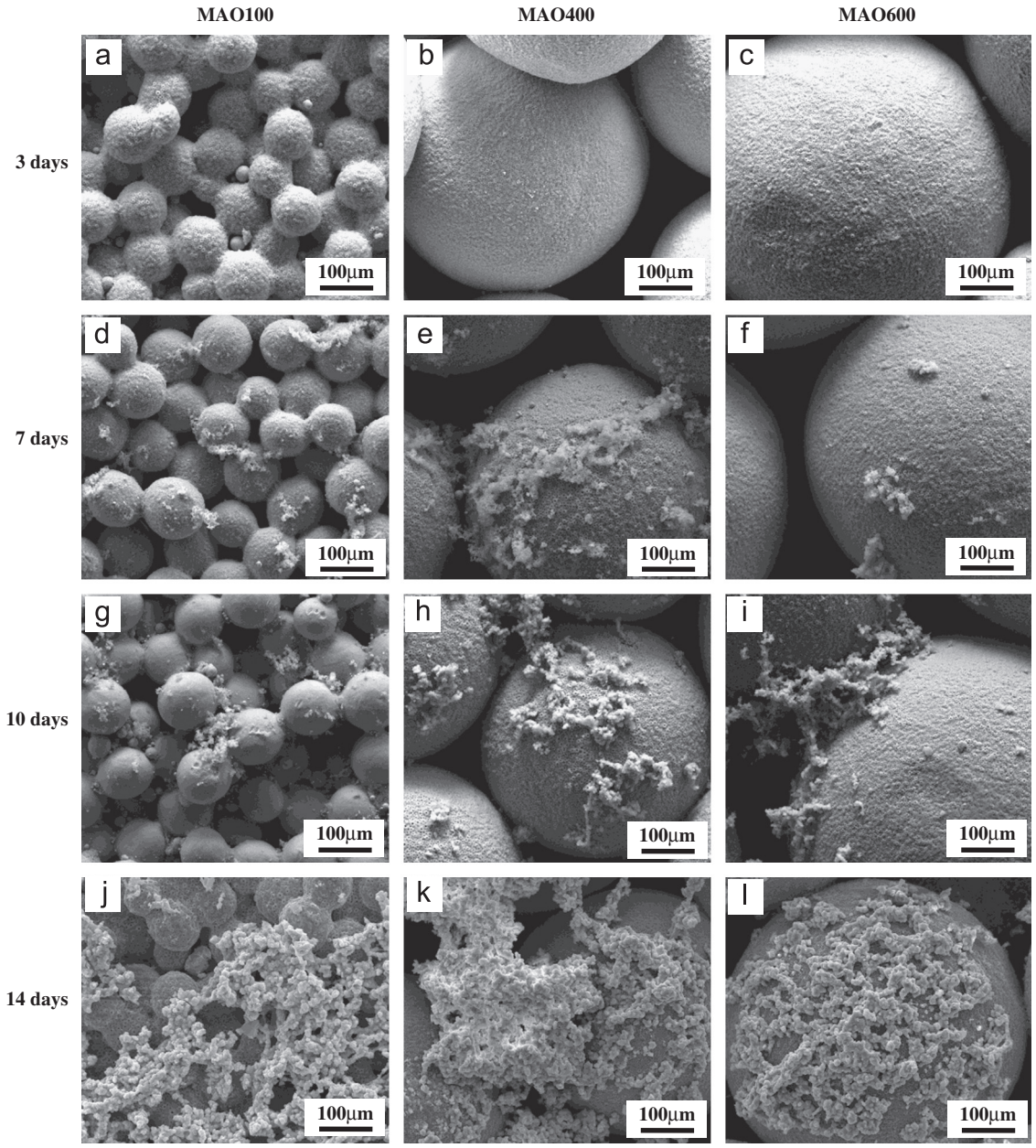

Fig. 10. SEM morphology of the MAO treated porous titanium after SBF immersion for 3, 7, 10 and 14 days: (a)–(c) MAO100, MAO400 and MAO600 for 3 days, (d)–(f) MAO100, MAO400 and MAO600 for 7 days, (g)–(i) MAO100, MAO400 and MAO600 for 10 days, (j)–(i) MAO100, MAO400 and MAO600 for 14 days.

treated porous titanium have apatite-forming ability. It can be clearly found that the intensity of apatite diffraction peaks is different as changing the titanium beads diameter, showing different apatite-forming capacities during the same time. And the relative intensity of apatite was improved with increasing the titanium beads diameter from 100 to 400 μm and then it decreased when the titanium beads diameter increased to 600 μm. This result indicated that the apatite formation ability of MAO400 coating is the highest among all MAO coatings.

The XRD and SEM results revealed that the MAO coatings could induce the formation of apatite, showing bioactivity. Apparently, the MAO coatings on different porous titanium with different titanium beads diameters show different apatite formation ability. Based on the previous research, the change of apatite formation ability is associated with the beads diameters as the different Si, Ca, P concentrations caused by varied oxidation ability during the MAO process.

Fig. 10 shows the SEM morphology of the MAO treated porous titanium after SBF immersion for 3, 7, 10 and 14 days. After SBF immersion for 3 days, no apatite deposition was observed on the surfaces of MAO100, MAO400 and MAO600. After SBF immersion for 7 days, apatite was formed on all coatings. And, the formation ability of apatite on the surface of MAO400 coating is highest according to SEM observation. When the SBF immersion time further increased, more apatite was found on the all surfaces of MAO coatings. However, the induction ability for apatite

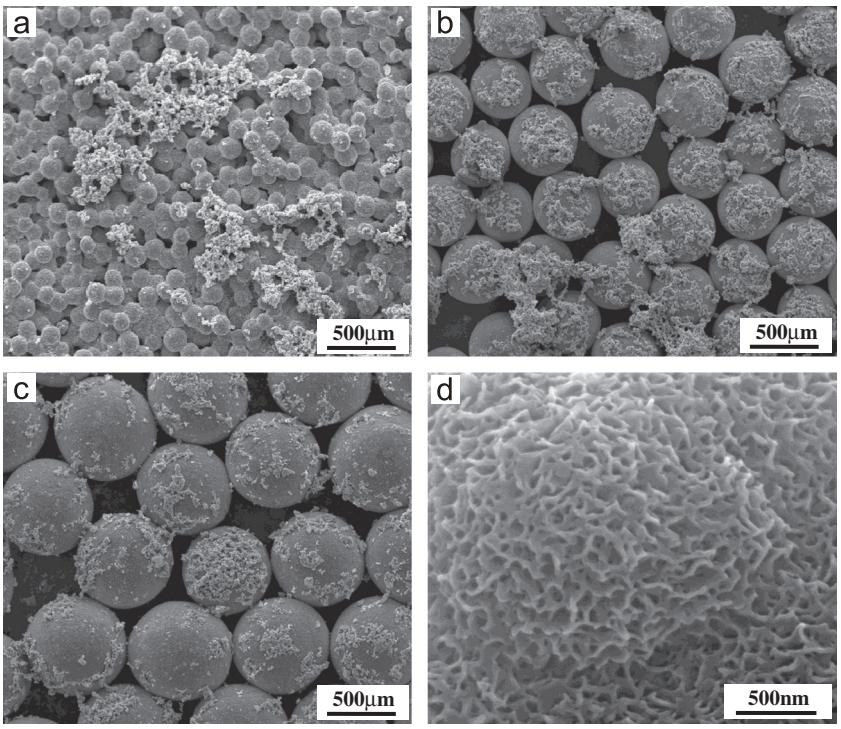

Fig. 11. SEM morphology of the MAO treated porous titanium after SBF immersion for 14 days: (a) MAO100, (b) MAO400, (c) MAO600, and (d) high magnification of (b).

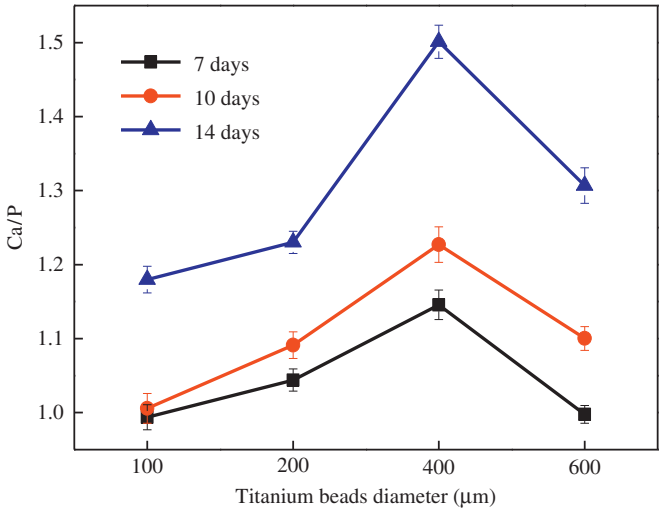

Fig. 12. The Ca/P ratio of apatite induced by MAO coatings on porous titanium for different SBF immersion time.

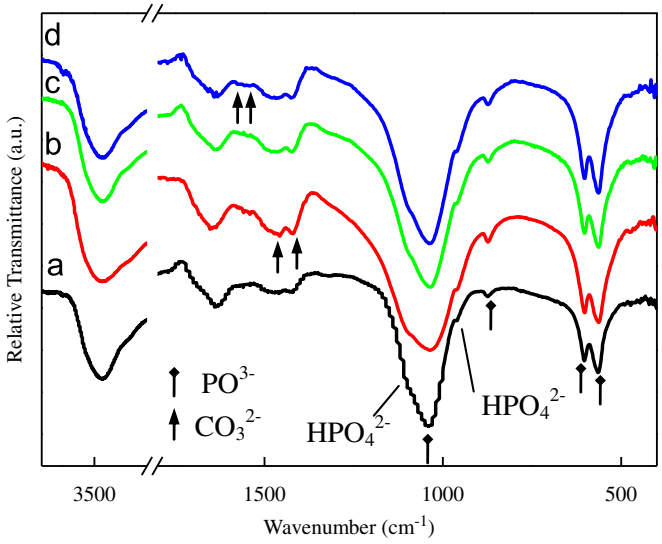

Fig. 13. FT-IR spectra of the MAO coating formed at the surface of porous titanium beads with different diameters after SBF immersion for 14 days: (a) MAO100, (b) MAO200, (c) MAO400, and (d) MAO600.

formation of MAO400 is always higher than any other MAO coatings according to SEM observation at a low magnification as shown in Fig.11. At high magnification, porous apatite products composed of nano scale apatite crystals were observed as shown in Fig. 11(d). Additionally, the apatite formation ability of MAO200 was between that of MAO100 and MAO400 (not shown here).

3.2.2. Ca/P ratio of apatite

Fig. 12 shows the Ca/P ratio of apatite induced by MAO coatings on porous titanium for different SBF immersion time. After SBF immersion for 7, 10 and 14 days, the Ca/P ratio of apatite induced by various MAO coatings on porous titanium increased firstly and then decreased with increasing the titanium beads diameter. Obviously, on all the MAO coatings, the Ca/P ratio of apatite was improved by increasing the SBF immersion time, displaying the continuous formation of apatite.

3.2.3. FT-IR analyze

Fig. 13 FT-IR spectra of the MAO coating formed at the surface of porous titanium beads with different diameters after

SBF immersion for 14 days. A broad absorption band at 3441 cm^{-1} and a bending mode at 1651 cm^{-1} indicate the presence of bonded water in the SBF incubated MAO coatings [32]. Absorption peaks of PO_4 bands were observed including the triply degenerated asymmetric stretching mode of ν_3PO_4 band at 1033 cm^{-1}, triply degenerated bending mode of ν_3PO_4 band at 602 and 566 cm^{-1} and double degenerated bending mode of ν_2PO^4 band at 471 cm^{-1} [32]. In addition, the FT-IR spectrum shows the CO_3^{2-}absorption bands of the characteristic stretching mode of $\nu 1CO_3^{2-}$ group in A-type slightly substituted carbonated-HA at 1462 cm^{-1}, stretching mode of $\nu 1CO_3^{2-}$ group in B-type slightly substituted carbonated-HA at 1421 cm^{-1} and bending mode of (ν_3 or v_4) CO_3^{2-} group in carbonated HA at 872 cm^{-1} [32]. Also, the HPO_4^{2-} groups were detected at characteristic peaks of 1099, 956 and 874 cm^{-1} [32]. The FT-IR result confirms that the apatite formed on the MAO coating has a carbonated structure.

4. Discussion

In this work, the chemical states of Ca, Si, Ti and O of MAO coatings on porous titanium formed by vacuum sintering titanium beads with different diameters were investigated. And formation and structure of apatite on various MAO coatings was further investigated. The effect of titanium beads diameter on the chemical states of Ca and Si of MAO coatings on the surfaces of porous titanium is not obvious. However, the chemical states of Ti and O changed when the titanium beads diameter increased.

The XPS results show the existence of low chemical state Ti^{2+}, indicating that the titanium surface could not be oxidized completely. Moreover, the content of Ti^{2+} decreased firstly and then increased according to Figs. 7 and 8, suggesting the oxidation ability on porous titanium also decreased firstly and then increased with increasing the titanium beads diameters. Correspondingly, high binding energy of O was observed due to the presence of Ti^{2+}. At the same time, the content of high binding energy of O decreased firstly and then increased with increasing the titanium beads diameters, according to Figs. 7 and 8. The previous research indicated that the porosity and specific surface area are two key factors to influence the formation and microstructures of MAO coatings. Associated considered the two parameters, as the oxidizing ability is negative correlated with bead diameter as porosity but positive correlated with bead diameter as specific surface area. Thus, the oxidizing ability first increased and then decreased with increasing the diameter of titanium beads due to the changes in porosity and specific surface area. When the oxidizing ability increased firstly and then decreased, obviously, the content of Ti^{2+} decreased firstly and then increased. In contrary, the change in content of high binding energy of O increased firstly and then decreased.

The current results reveal that the MAO coatings containing SCN elements have good induction capability for the heterogeneous nucleation and growth of apatite in the SBF. The contribution of the SCN elements for the bioactivity is significant in various bioactive inorganic compounds such as bioactive glasses–ceramics, which can bond to bone tissues well because it can induce a layer of biologically active hydroxycarbonate apatite spontaneously under a physiological environment due to the presence of Si, Ca and Na, etc. Generally, bonelike apatite formation on biomaterial surface in SBF requires a chemical stimulus. The apatite-bonding structure is highly dependent on the chemical reactivity of the materials surface in fluids. In this work, the formation of apatite could be explained as following according to the current and previous research [33]. Firstly, the deposition of apatite could be related with the formation of hydrated silica gel layer on the surfaces based on the previous researches [33], which could provide the chemical stimulus for the apatite deposition. The formation of hydrated silica gel is via dissolution of Na^+ ion from the surface based on the previous researches [33]. Moreover, the dissolution of Ca^{2+} ion into the SBF could also act as similar effect on the formation of OH group compared to Na^+ ion. At the same time, the dissolution of Ca^{2+} ion could further increase the local supersaturation near the surface of MAO coatings, promoting the deposition of calcium phosphates. Based on the above discussion, the concentrations of the Si, Ca of the MAO coatings increased, then the apatite formation ability of the MAO coatings could be improved. From the current results, it was found the concentrations of the Si, Ca of the MAO coatings on the porous titanium increased firstly and then decreased with increasing the titanium beads diameters.

The apatite structure is very hospitable in allowing the substitutions of many other ions. The biomimetic apatite formed in SBF is similar to synthetic HA, but they differ from HA in composition, stoichiometry, and physical and mechanical properties. In fact, most investigations indicated that biomimetic apatites possess relative low Ca/P ratios due to the lack of Ca^{2+} ions in the apatite crystal, since the Ca^{2+} ions could be substituted by K^+, Na^+ and Mg^{2+} ions, and the PO_4^{3-} and OH^- groups could be substituted by HPO_4^{2-}, CO_3^{2-}, Cl^- and F^- ions based on the Fig. 12 and previous research [33]. According to the EDS results, a small quantity of Na and Mg was detected in the apatite layers (not shown here).

5. Conclusion

The microarc oxidized TiO_2 based coating containing Si, Ca and Na elements (SCN) were formed on porous titanium sintered with different sizes of titanium beads. The titanium beads diameter does not affect the chemical states of Ca and Si of MAO coatings on the surfaces of porous titanium. However, the chemical states of Ti and O changed when the titanium beads diameter increased. The MAO coatings have good induction capability due to the introduction of SCN elements. And, the A-type slightly substituted carbonated-HA and B-type slightly substituted carbonated-HA with HPO_4^{2-} group were obtained after immersion of the MAO coatings in SBF. The appropriate size of titanium beads can be important to introduce more amounts of SCN elements into MAO coatings on the porous titanium, which results in a high apatite-formation ability

of MAO coatings on porous titanium with appropriate size of titanium beads.

Acknowledgments

This work was financially supported by the National Natural Science Foundation of China (Grant nos. 51002039 and 51021002), Fund for the Doctoral Project to new teachers, National Basic Science Research Program (2012CB933900), the Fundamental Research Funds for the Central Universities (Grant no. HIT.NSRIF.2014002).

References

[1] J.P. Li, P. Habibovic, M. van den Doel, C.E. Wilson, J.R. de Wijn, C.A. van Blitterswijk, K. de Groot, Bone ingrowth in porous titanium implants produced by 3D fiber deposition, Biomaterials 28 (2007) 2810–2820.

[2] M.C. Melican, M.C. Zimmerman, M.S. Dhillon, A.R. Ponnambalam, A. Curodeau, J.R. Parsons, Three-dimensional printing and porous metallic surfaces: a new orthopedic application, Journal of Biomedical Materials Research 55 (2001) 194–202.

[3] G. Ryan, A. Pandit, D.P. Apatsidis, Fabrication methods of porous metals for use in orthopaedic applications, Biomaterials 27 (2006) 2651–2670.

[4] K.H.W. Seah, R. Thampuran, S.H. Teoh, The influence of pore morphology on corrosion, Corrosion Science 40 (1998) 547–556.

[5] Y. Okazaki, E. Nishimura, H. Nakada, Surface analysis of Ti–15Zr–4Nb–4Ta alloy after implantation in rat tibia, Biomaterials 22 (2001) 599–607.

[6] I.H. Oh, N. Nomura, N. Masahashi, S. Hanada, Mechanical properties of porous titanium compacts prepared by powder sintering, Scripta Materialia 49 (2003) 1197–1202.

[7] G.A. Murray, J.C. Semple, Transfer of tensile loads from a prosthesis to bone using porous titanium, Journal of Bone andJoint Surgery(British) 63-B (1981) 138–141.

[8] M. Bram, C. Stiller, H.P. Buchkremer, D. Stover, H. Baur, High-porosity titanium, stainless steel, and superalloy parts, Advanced Engineering Materials 2 (2000) 196–199.

[9] C.E. Wen, M. Mabuchi, Y. Yamada, K. Shimojima, Y. Chino, T. Asahina, Processing of biocompatible porous Ti and Mg, Scripta Materialia 45 (2001) 1147–1153.

[10] B. Gorny, T. Niendorf, J. Lackmann, M. Thoene, T. Troester, H.J. Maier, In situ characterization of the deformation and failure behavior of non-stochastic porous structures processed by selective laser melting, Materials Science and Engineering: A 528 (2011) 7962–7967.

[11] L. Markus, H. Simon, M. Wilhelm, W. Konrad, S. Ralf, T. Rainer, P. Reinhart, F. Horst, Manufacturing of individual biodegradable bone substitute implants using selective laser melting technique, Journal of Biomedical Materials Research Part A 97A (2011) 466–471.

[12] H. Nikolas, H. Peter, F. Brian, K. Carolin, B. Rajendra, Compression–compression fatigue of selective electron beam melted cellular titanium (Ti-6Al-4V), Journal of Biomedical Materials Research Part B 99B (2011) 313–320.

[13] D.A. Puleo, R.A. Kissling, M.S. Sheu, A technique to immobilize bioactive proteins, including bone morphogenetic protein-4 (BMP-4), on titanium alloy, Biomaterials 23 (2002) 2079–2087.

[14] K. Das, S. Bose, Surface modifications and cell–materials interactions with anodized Ti, Acta Biomaterialia 3 (2007) 573–585.

[15] X.Y. Liu, P.K. Chu, C.X. Ding, Surface modification of titanium, titanium alloys, and related materials for biomedical applications, Materials Science and Engineering R: Reports 47 (2004) 49–121.

[16] D. Sreekanth, N. Rameshbabu, K. Venkateswarlu, Effect of various additives on morphology and corrosion behavior of ceramic coatings developed on AZ31 magnesium alloy by plasma electrolytic oxidation, Ceramics International 38 (2012) 4607–4615.

[17] Y.M. Wang, B.L. Jiang, T.Q. Lei, L.X. Guo, Microarc oxidation coatings formed on Ti6Al4V in Na_2SiO_3 system solution: microstructure, mechanical and tribological properties, Surface and Coatings Technology 201 (2006) 82–89.

[18] A. Ghasemi, V.S. Raja, C. Blawert, W. Dietzel, K.U. Kainer, The role of anions in the formation and corrosion resistance of the plasma electrolytic oxidation coatings, Surface and Coatings Technology 204 (2010) 1469–1478.

[19] Y.L. Cheng, F. Wu, E. Matykina, P. Skeldon, G.E. Thompson, The influences of microdischarge types and silicate on the morphologies and phase compositions of plasma electrolytic oxidation coatings on Zircaloy-2, Corrosion Science 59 (2012) 307–315.

[20] Y.M. Wang, D.C. Jia, L.X. Guo, T.Q. Lei, B.L. Jiang, Effect of discharge pulsating on microarc oxidation coatings formed on Ti6Al4V alloy, Materials Chemistry and Physics 90 (2005) 128–133.

[21] F. Liu, F.P. Wang, T. Shimizu, K. Igarashi, L.C. Zhao, Hydroxyapatite formation on oxide films containing Ca and P by hydrothermal treatment, Ceramics International 32 (2006) 527–531.

[22] Y.K. Pan, C.Z. Chen, D.G. Wang, X. Yu, Z.Q. Lin, Influence of additives on microstructure and property of microarc oxidized Mg–Si–O coatings, Ceramics International 38 (2012) 5527–5533.

[23] X.L. Zhu, J.L. Ong, S. Kim, K. Kim, Surface characteristics and structure of anodic oxide films containing Ca and P on a titanium implant material, Journal of Biomedical Materials Research Part B 60B (2002) 333–338.

[24] X.L. Zhu, K.H. Kim, Y.S. Jeong, Anodic oxide films containing Ca and P of titanium biomaterial, Biomaterials 22 (2001) 2199–2206.

[25] D.Q. Wei, Y. Zhou, D.C. Jia, Y.M. Wang, Characteristic and in vitro bioactivity of a microarc-oxidized TiO_2-based coating after chemical treatment, Acta Biomaterialia 3 (2007) 817–827.

[26] S. Cheng, D.Q. Wei, Y. Zhou, H.F. Guo, Preparation, cell response and apatite-forming ability of microarc oxidized coatings containing Si, Ca and Na on titanium, Ceramics International 37 (2011) 2505–2512.

[27] S. Cheng, D.Q. Wei, Y. Zhou, H.F. Guo, Characterization and properties of microarc oxidized coatings containing Si, Ca and Na on titanium, Ceramics International 37 (2011) 1761–1768.

[28] R. Zhou, D.Q. Wei, S. Cheng, Y. Zhou, D.C. Jia, Y.M. Wang, B.Q. Li, The effect of titanium bead diameter of porous titanium on the formation of micro-arc oxidized TiO_2-based coatings containing Si and Ca, Ceramics International 39 (2013) 5725–5732.

[29] A. Oyane, H.M. Kim, T. Furuya, T. Kokubo, T. Miyazaki, T. Nakamura, Preparation and assessment of revised simulated body fluids, Journal of Biomedical Materials Research Part A 65A (2003) 188–195.

[30] W.H. Song, Y.K. Jun, Y. Han, S.H. Hong, Biomimetic apatite coatings on micro-arc oxidized titania, Biomaterials 25 (2004) 3341–3349.

[31] B.D. Ng, I. Annergren, A.M. Soutar, K.A. Khor, A.E.W. Jarfors, Characterisation of a duplex TiO_2/CaP coating on Ti6Al4V for hard tissue replacement, Biomaterials 26 (2005) 1087–1095.

[32] L. Müller, F.A. Müller, Preparation of SBF with different HCO_3- content and its influence on the composition of biomimetic apatites, Acta Biomaterialia 2 (2006) 181–189.

[33] S. Hayakawa, K. Tsuru, C. Ohtsuki, A. Osaka, Mechanism of apatite formation on a sodium silicate glass in a simulated body fluid, Journal of the American Ceramic Society 82 (1999) 2155–2160.